Energy & Environmental Science

COMMUNICATION

View Article Online
View Journal | View Issue

Cite this: *Energy Environ. Sci.*, 2014, 7, 2619

Received 11th April 2014
Accepted 19th May 2014

DOI: 10.1039/c4ee01138d

www.rsc.org/ees

Efficient, high yield perovskite photovoltaic devices grown by interdiffusion of solution-processed precursor stacking layers†

Zhengguo Xiao,‡[a] Cheng Bi,‡[a] Yuchuan Shao,[a] Qingfeng Dong,[a] Qi Wang,[a] Yongbo Yuan,[a] Chenggong Wang,[b] Yongli Gao[bc] and Jinsong Huang*[a]

We report on an interdiffusion method to fabricate pin-hole free perovskite films using a low temperature (<105 °C) solution process. A high efficiency of 15.4%, with a fill factor of ~80%, was achieved for the devices under one sun illumination. The interdiffusion method results in high device yield, with an efficiency of above 14.5% for more than 85% of the devices.

Organometal trihalide perovskites are emerging as a new generation of solution processable, low cost photovoltaic materials which are abundant in nature. A high power conversion efficiency of around 15% has been achieved in both mesoporous structure devices as well as planar heterojunction (PHJ) devices.[1–17] In addition to the strong absorption in the ultraviolet visible range, organometal trihalide perovskites have intriguing optoelectronic properties, such as excellent crystallinity, very large carrier mobility comparable to silicon, bipolar transport, and large charge diffusion length which enable high performance devices with the traditional PHJ structure.[2,7,12,14,15,17] In addition to the simple device structure, PHJ perovskite devices have been demonstrated to have better stability under ultraviolet (UV) light by removing mesoporous TiO_2, which causes instability due to the UV light-induced desorption of surface-adsorbed oxygen.[18] Recent studies demonstrate that a dual source vacuum sublimation technique produces a homogeneous and densely packed perovskite film.[2,19] However, depositing a continuous, leakage-free perovskite film with a thickness comparable to the charge diffusion length using solution processes has proven to be very difficult.[2,7,17,20,21] Noncontinuous perovskite films were frequently observed using lead iodine (PbI_2) and methyl ammonium halide (CH_3NH_3X, or MAX) blend solutions, which might be related to the interaction of the perovskite with a substrate surface.[17,20] Our recent observations indicate that it may also be due to the low viscosity of the perovskite solution and the quick crystallization of the mixed precursor upon drying the spun films.[22] The power conversion efficiency (PCE) of low-temperature solution-processed perovskite devices in the range of 4–12% was far below those of devices with a mesoporous structure or fabricated by thermal evaporation.[2,4,17]

In this manuscript, we report a method of forming continuous, compact iodine perovskite ($MAPbI_3$) films by interdiffusion of spin-coated stacking layers of PbI_2 and MAI. The high quality film achieved allows the fabrication of leakage-free photovoltaic devices with a high PCE of 15.4% under one sun and 17.0% under 0.03 sun illumination.

The deposition and thermal annealing processes of the PbI_2/MAI stacking layer films are illustrated in Fig. 1a. For the film fabrication, PbI_2 and MAI were first dissolved in dimethylformamide (DMF) and 2-propanol, respectively, as precursor solutions at varied concentrations. The precursors were then spun onto poly(3,4-ethylenedioxythiophene):poly(styrenesulphonate) (PEDOT:PSS) covered indium tin oxide (ITO) glass with a PbI_2 layer underneath an MAI layer. A supersaturated hot solution of PbI_2 was used for quick drying to obtain a pin-hole free and conformal PbI_2 layer on the PEDOT:PSS surface. Since PbI_2 has relatively low solubility in 2-propanol, the spin coating of MAI did not wash off the PbI_2. The bilayer films were then annealed at a temperature of 100 °C for varied durations. The scanning electron microscopy (SEM) picture in Fig. 1b reveals a very continuous PbI_2 film, which is uncommon for an inorganic salt. The dried PbI_2/MAI bilayer films are rougher than PbI_2 layers due to the formation of $MAPbI_3$ microcrystals upon drying and thermal annealing. Nevertheless, they are still continuous and pinhole free across the whole device area, as shown by the large area SEM image in Fig. 1c. More detailed procedures of the

[a]Department of Mechanical and Materials Engineering, Nebraska Center for Materials and Nanoscience, University of Nebraska-Lincoln, Lincoln, Nebraska 68588-0656, USA. E-mail: jhuang2@unl.edu

[b]Department of Physics and Astronomy, University of Rochester, Rochester, NY 14627, USA

[c]Institute of Super-microstructure and Ultrafast Process in Advanced Materials (ISUPAM), Central South University, Changsha, Hunan, People's Republic of China 410083

† Electronic supplementary information (ESI) available. See DOI: 10.1039/c4ee01138d

‡ Z. X. and C. B. contributed to this work equally.

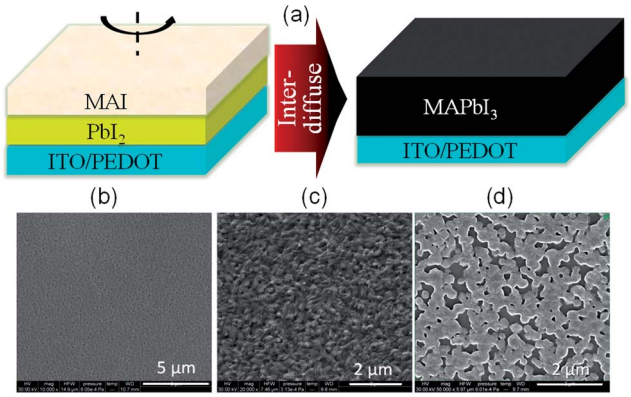

Fig. 1 (a) Schematics of spin coating of PbI_2 and MAI using orthogonal solvents and the conversion of the stacking layer into a perovskite layer upon annealing. The SEM image of the PbI_2 film (b), the annealed perovskite layer formed by an interdiffusion process (c), and the annealed perovskite film spun from the premixed PbI_2 and MAI solution (d).

perovskite film fabrication can be found in the ESI.† In contrast, the $MAPbI_3$ films spun from premixed PbI_2 and MAI blend solutions generally are nonuniform with many microstructures on the surface, as shown in Fig. 1d.[22]

We studied the interdiffusion process of PbI_2 and MAI stacking layers. A thickness ratio of 1.4 : 1 for the MAI : PbI_2 layer, calculated from the density and molecular weight, is needed to form a stoichiometry iodine perovskite by assuming a complete interdiffusion and reaction of the precursors. The thickness of the PbI_2 layer was varied from 40 nm to 200 nm, and the thickness of MAI varied from 60 nm to 250 nm by controlling the concentration of the precursor solutions and the spin rate, which are summarized in Table S1.† There is a quick reaction of MAI and PbI_2 upon contact, evidenced by the immediate color change of the bilayer films observed right after the spin coating of the MAI layer, which is consistent with previous observations in mesoporous structure devices[1] Fig. 2a

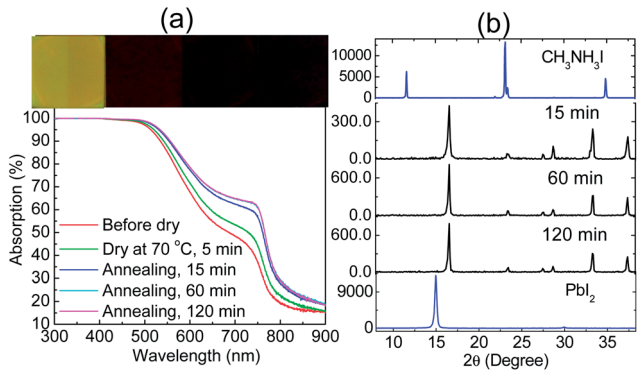

Fig. 2 (a) Single-path absorption of the perovskite film after dry and at various annealing durations. The inset shows the pictures, from left to right, of the spun PbI_2 film, the PbI_2/MAI film before drying, the PbI_2/MAI films after drying, and after 15 min of annealing; (b) the XRD pattern of MAI, PbI_2, and the perovskite films formed by interdiffusion at varied annealing times.

shows the evolution of the color change of the films at different stages.

The interdiffusion of the PbI_2/MAI films and the formation of perovskites after varied annealing times were studied by absorption spectra and X-ray diffraction (XRD). Fig. 2a shows typical absorption spectra of a PbI_2/MAI stacking film after different annealing durations from 0 min to 2 h at a temperature of 100 °C. The absorption at a wavelength of around 740 nm from the perovskite quickly increased during the first 15 min of thermal annealing and then saturated after 1 h of annealing. The XRD patterns *versus* time of these films have the same variation trend with absorption spectra. As shown in Fig. 2b, both MAI and PbI_2 peaks disappear after 15 min of annealing and remain almost unchanged afterwards. No impurity peak was identified from XRD patterns. This indicates that the long-range interdiffusion of MAI and PbI_2 occurs primarily during the first 15 min of annealing.

It should be noted that the interdiffusion approach reported here is very different from the sequential deposition method reported by *Burschka et al.*[1] which makes good mesoporous structure perovskite solar cells but not PHJ ones. We dipped a 140 nm PbI_2 film into MAI solution; however, we obtained very non-uniform, rough perovskite films, as shown in Fig. S1.† The efficiency of the devices based on these films only reached 3.2%. The low performance can be explained by the difficulty of MAI to penetrate into the thick PbI_2 films, and the quick crystallization of perovskite yielded many large randomly distributed grains, which resulted in a very rough perovskite film. Another difference is that the thermal annealing process is required in the interdiffusion method reported here to make sure that the compact PbI_2 can be fully reacted with MAI. In the mesoporous perovskite photovoltaic devices with porous TiO_2 structures,[1] PbI_2 absorbed onto TiO_2 can be much thinner because of the very large surface area of the mesoporous structure needed to absorb enough PbI_2. Due to the very thin PbI_2 in a mesoporous structure, the reaction of PbI_2 and MAI can be very quick and complete without resorting to thermal annealing. However, for the spun compact PbI_2 and MAI stacking layers, there is still unreacted MAI and PbI_2 right after deposition, shown by the SEM image of the as-prepared PbI_2 and MAI stacking layers in Fig. S2.† The devices made of such films show a low PCE, below 1%, with a typical S-shaped photocurrent, a signature of large series resistance caused by the insulating MAI and/or PbI_2. A thermal annealing is thus still needed to drive the interdiffusion of MAI and PbI_2, which can be visually observed by the increased darkness of the $MAPbI_3$ films.

The devices have a structure of ITO/PEDOT:PSS/$MAPbI_3$/[6,6]-phenyl-C61-butyric acid methyl ester (PCBM 20 nm)/C_{60}/(20 nm)/2,9-dimethyl-4,7-diphenyl-1,10-phenanthroline (BCP, 8 nm)/aluminium (Al, 100 nm). A cross-sectional SEM of the whole device is shown in Fig. 3a which shows a continuous, pin-hole free perovskite formed on PEDOT:PSS with a film thickness variation of less than 20 nm. Secondary ion mass spectrometry (SIMS) measurements on the real device without an Al electrode, as shown in Fig. 3b, revealed a layered structure and the penetration of Pb^{2+} and I^- across the whole perovskite layer. The depth composition profile of Pb^{2+}

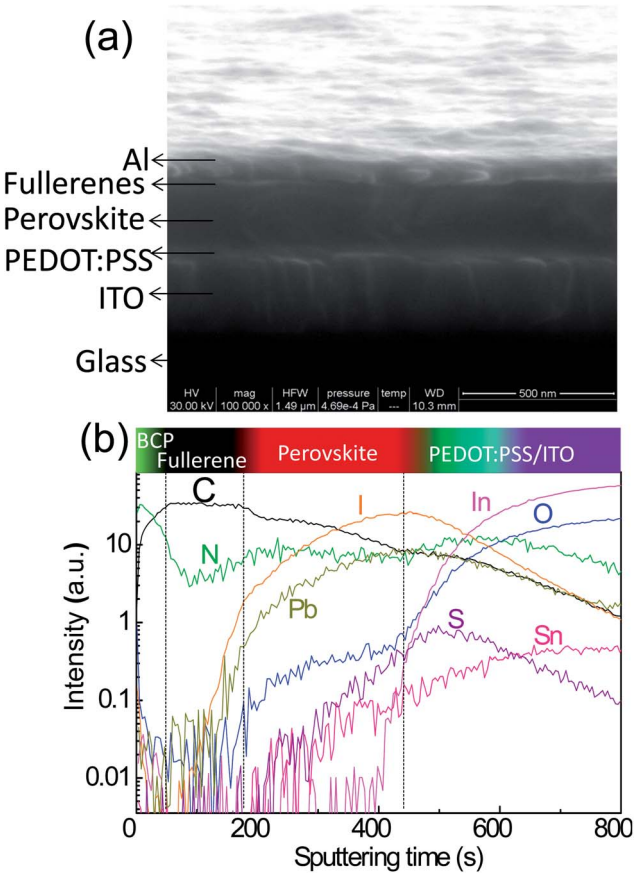

Fig. 3 (a) Cross-sectional SEM image of the best-performing perovskite device. The scale bar is 500 nm. The thickness of the perovskite layer is ~270 nm; (b) composition depth profiles of the device without the Al electrode measured by SIMS.

and I^- shows a graded composition with increased Pb^{2+} and I^- toward the PEDOT:PSS side, which might be caused by the incomplete diffusion of traceable PbI_2 to the surface but most likely by nonuniform sputtering of the perovskite layer. Nevertheless the deficiency of Pb^{2+} on the top surface of these perovskite films was also observed by X-ray photoelectron spectroscopy measurements, as summarized in Table S2.† Hall effect measurements reveal a p-type perovskite and a low extrinsic hole concentration of around 4–10 $\times$ 10^{13} cm^{-3}, which might be due to the Pb deficiency in the perovskite films formed by the interdiffusion approach in which there is excess MAI supply.[23]

In our devices, a PCBM layer spun onto the perovskite layer followed by thermal annealing is used to passivate the perovskite surface and grain boundaries.[24] Hall effect measurements have shown that PCBM passivation can reduce the extrinsic hole concentration caused by unintentional doping in solution-processed perovskites by three times and improve the carrier mobility by three times. The additional C_{60} layer further passivates perovskite films and reduces the trap state density.[22] The device performance is very sensitive to the precursor thickness ratio, thermal annealing time, and perovskite thickness. The unmatched PbI_2 or MAI thickness always results in reduced short circuit current density (J_{SC}) and fill factor (FF), which might be caused by the traceable insulating precursors or nonstoichiometric compounds.

Fig. 4a shows typical photocurrents of the devices with a fixed PbI_2 thickness (140 nm) and varied MAI thicknesses, demonstrating how the device performance was optimized. Fig. 4b shows the photocurrents of the devices with varied perovskite thicknesses varied from 200 nm to 320 nm. It is clear that a thicker perovskite film absorbs more light and thus yields a larger photocurrent, while a too-large thickness causes loss of photovoltage, most likely due to the increased charge recombination. The optimized $MAPbI_3$ devices have a perovskite thickness of 270–300 nm which is twofold longer than that of the previously measured low end of the electron and hole diffusion length of around 100–130 nm.[12,14] The long carrier extraction length should be ascribed to the excellent crystallinity, passivation by fullerenes,[24] and/or low extrinsic doping of perovskite films formed by interdiffusion. It demonstrates the advantages of the interdiffusion approach in the formation of high quality perovskite films. The highest PCE devices were obtained by annealing of PbI_2/MAI with a thickness of 140/190 nm at 100 °C for 2 hours. The device was measured under AM 1.5 simulated one sun illumination.

The device area is 9.6 mm^2, determined by the overlap of the cathode and anode electrodes. In order to avoid the overestimation of the photocurrent density by the piping effect, an aperture size of 8 mm^2 was used to define the light absorption area.[25] A Schott KG5 color-filtered Si diode (Hamamatsu S1133) was used to calibrate the light intensity of the solar simulator before photocurrent measurements to avoid optical mismatch.[26]

The best performing device has a J_{SC} of 19.6 mA cm^{-2}, a FF of 79.3%, an open circuit voltage (V_{OC}) of 0.99 V, and a PCE of 15.4%. Fig. 4c shows the external quantum efficiency (EQE) of the device. The calculated J_{SC} from the EQE spectra is 18.9 mA cm^{-2}, which is close to the measured J_{SC} of 19.6 mA cm^{-2}. It is noted that there are two troughs in the EQE spectrum at around 400 nm and 600 nm, which is caused by the stronger reflection of the glass/ITO substrates at these wavelength regions. Another best performing device with larger photocurrent but smaller V_{OC} shows an even higher efficiency of 16–17% at a lower light intensity of 3.2–30 mW cm^{-2}, as summarized in Table 1. The light intensity was tuned by applying neutral density filters of different optical densities. The higher efficiency under lower light intensity is ascribed to the reduced charge recombination evidenced by the larger FF, up to 82%. There is still room to further increase the carrier diffusion length for efficiency enhancement. Although a larger J_{SC} of 22 mA cm^{-2} could be reached in our devices with thicker perovskites , the V_{OC} and FF generally reduce, pulling down the PCE, which still needs a thorough understanding on the charge recombination process in perovskite materials and electrode interfaces to recover the V_{OC} and FF.

One significant improvement of the device performance reported in this work is the large FF of around 80% for most of our devices. The statistics of the FF, J_{SC}, and V_{OC} are shown in Fig. 4d–f. In addition to the reduced charge recombination in perovskite layers due to their good crystallinity and passivation by PCBM, both at the top surface and at the grain boundaries inside the perovskite films,[24] the compact and leakage-free

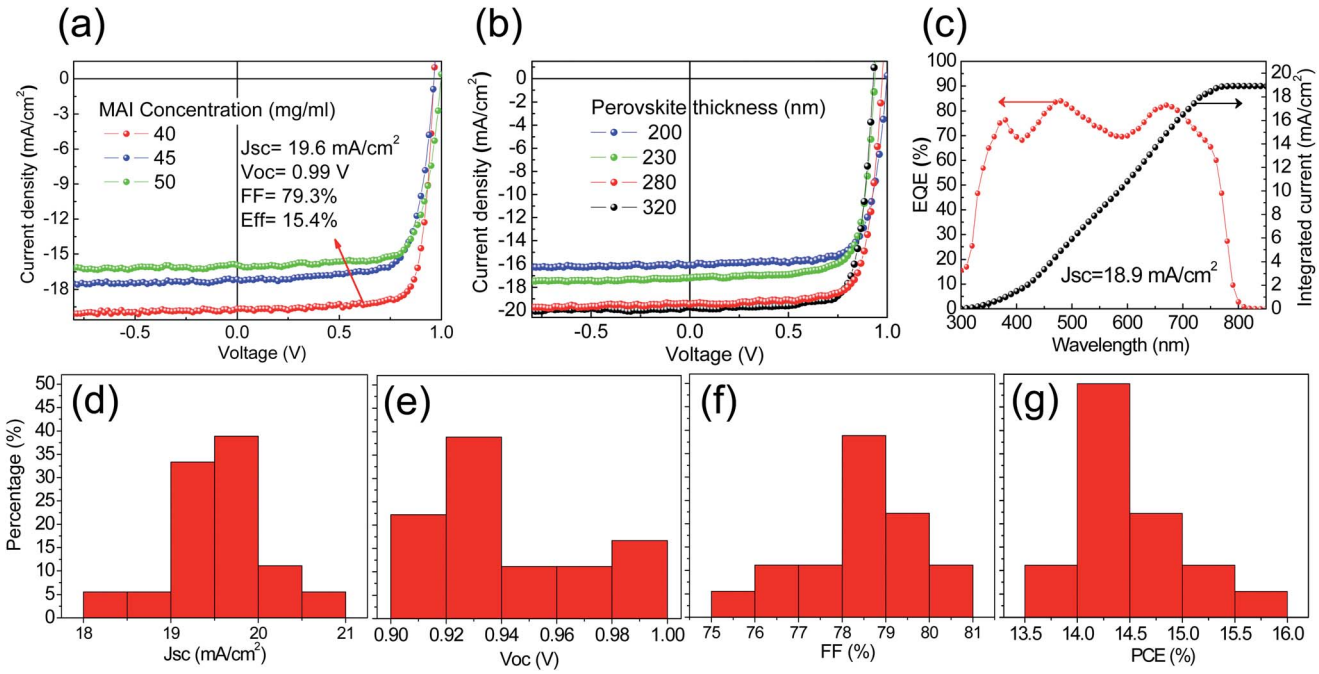

Fig. 4 Performance of the perovskite devices. (a) Photocurrents of the device with a PbI_2 thickness of 140 nm while varied MAI concentrations from 40–50 mg ml^{-1}; (b) Photocurrents of the devices with perovskite films of different thickness varied from 200 to 320 nm; (c) external quantum efficiency of one optimized device. (d–g) Device performance statistics based on more than 50 devices from five batches.

Table 1 Photovoltaic performance of a best-performing device under different illumination light intensities

Light intensity (mW cm^{-2})	J_{SC} (mA cm^{-2})	V_{OC} (V)	FF (%)	PCE (%)
3.20	0.78	0.85	82.2	17.0
31	7.09	0.92	77.0	16.2
100	20.59	0.94	78.8	15.3

perovskite films formed by the interdiffusion process should also contribute to the large FF. Most of the devices have a low saturated dark current density in the order of 10^{-4} to 10^{-3} mA cm^{-2} at −2 V. The 15.4% device has a large shunt resistance of 4.67 kΩ cm^2 and a small series resistance of 1.06 Ω cm^2 calculated from the photocurrent curve which is among the best values reported. Another merit of the interdiffusion method for fabricating perovskite devices is that it gives an excellent yield of high PCE devices which is attractive for a large-scale production of perovskite devices. The statistics of the PCE based on more than 50 devices from five batches are shown in Fig. 4g. The average PCE is 14.5% and 85% of the devices have an efficiency of above 14%.

It has been reported that photocurrent hysteresis appears in some perovskite devices, which is strongly dependent on the device fabrication process as well as the measurement of

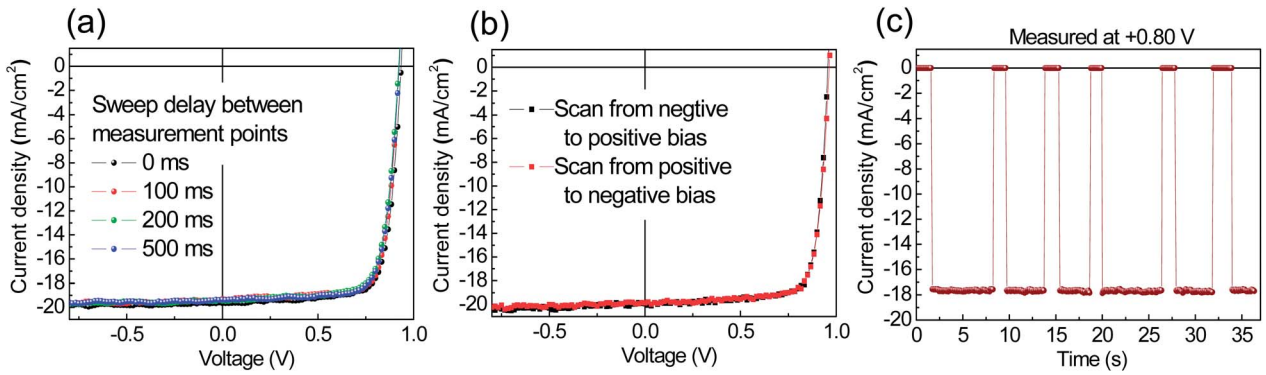

Fig. 5 (a) Photocurrents of a high performance perovskite device measured with different delays between measurement points (a) and different sweep directions (b). No obvious hysteresis of photocurrent was observed. (c) Measured photocurrent output at the maximum power point of a high performance device *versus* time by turning on and off the illumination with a chopper.

scanning rate and directions.[27] The origin of photocurrent hysteresis was ascribed to either the traps, ferroelectric properties of the perovskite material and/or the electromigration of ions in the perovskites. Here we changed the scanning rate from very fast to very slow, with a delay between measurement voltage points increased from 0 to 500 ms, which corresponds to the scan rate of 10.4 V s^{-1} to 0.033 V s^{-1}. The slowest scanning rate is comparable to what *Snaith et al.* reported.[27] As shown in Fig. 5a and b, no obvious hysteresis of photocurrent was observed by changing the sweep rates or the direction in our devices or the sweep rates. This indicates that the origin of hysteresis in photocurrent is more likely due to the trap formation in some nonoptimized films and device fabrication processes. The ultimate way to examine the efficiency of a solar cell device is to measure its power output at the load point. If there is large density of traps in the devices or photocurrent hysteresis for other reasons, the photocurrent would rise slowly upon turning on illumination. Fig. 5c shows that the photocurrent rose quickly to maximum on the timescale limited by the spin rate of the chopper, proving the presence of a negligible amount of charge traps in our optimized devices.

Conclusions

The interdiffusion method can be simply applied to other types of perovskite materials for incorporating Cl, Br, F, or other elements into precursor solutions and can also start with thermally evaporated precursor stacking layers to relieve the strict requirements for composition controlling in the co-evaporation process. The low temperature used is compatible with plastic flexible substrates. The interdiffusion approach can be potentially scaled up for large area device fabrication with established solution-process techniques, such as die-slot coating, gravure coating, and doctor blade coating.

Notes and references

1 J. Burschka, N. Pellet, S.-J. Moon, R. Humphry-Baker, P. Gao, M. K. Nazeeruddin and M. Grätzel, *Nature*, 2013, **499**, 316.
2 M. Liu, M. B. Johnston and H. J. Snaith, *Nature*, 2013, **501**, 395.
3 A. Kojima, K. Teshima, Y. Shirai and T. Miyasaka, *J. Am. Chem. Soc.*, 2009, **131**, 6050.
4 M. M. Lee, J. Teuscher, T. Miyasaka, T. N. Murakami and H. J. Snaith, *Science*, 2012, **338**, 643.
5 A. Abrusci, S. D. Stranks, P. Docampo, H.-L. Yip, A. K. Y. Jen and H. J. Snaith, *Nano Lett.*, 2013, **13**, 3124.
6 J. M. Ball, M. M. Lee, A. Hey and H. J. Snaith, *Energy Environ. Sci.*, 2013, **6**, 1739.
7 G. Hodes, *Science*, 2013, **342**, 317.
8 J. Y. Jeng, Y. F. Chiang, M. H. Lee, S. R. Peng, T. F. Guo, P. Chen and T. C. Wen, *Adv. Mater.*, 2013, **25**, 3727.
9 H.-S. Kim, I. Mora-Sero, V. Gonzalez-Pedro, F. Fabregat-Santiago, E. J. Juarez-Perez, N.-G. Park and J. Bisquert, *Nat. Commun.*, 2013, **4**, 2242.
10 N.-G. Park, *J. Phys. Chem. Lett.*, 2013, **4**, 2423.
11 H. J. Snaith, *J. Phys. Chem. Lett.*, 2013, **4**, 3623.
12 S. D. Stranks, G. E. Eperon, G. Grancini, C. Menelaou, M. J. Alcocer, T. Leijtens, L. M. Herz, A. Petrozza and H. J. Snaith, *Science*, 2013, **342**, 341.
13 W. Zhang, M. Saliba, S. D. Stranks, Y. Sun, X. Shi, U. Wiesner and H. J. Snaith, *Nano Lett.*, 2013, **13**, 4505.
14 G. Xing, N. Mathews, S. Sun, S. S. Lim, Y. M. Lam, M. Grätzel, S. Mhaisalkar and T. C. Sum, *Science*, 2013, **342**, 344.
15 J. H. Heo, S. H. Im, J. H. Noh, T. N. Mandal, C.-S. Lim, J. A. Chang, Y. H. Lee, H.-J. Kim, A. Sarkar and M. K. Nazeeruddin, *Nat. Photonics*, 2013, **7**, 486.
16 N.-G. Park, *J. Phys. Chem. Lett.*, 2013, **4**, 2423.
17 P. Docampo, J. M. Ball, M. Darwich, G. E. Eperon and H. J. Snaith, *Nat. Commun.*, 2013, **4**, 2761.
18 T. Leijtens, G. E. Eperon, S. Pathak, A. Abate, M. M. Lee and H. J. Snaith, *Nat. Commun.*, 2013, **4**, 2885.
19 O. Malinkiewicz, A. Yella, Y. H. Lee, G. M. Espallargas, M. Graetzel, M. K. Nazeeruddin and H. J. Bolink, *Nat. Photonics*, 2014, **8**, 128.
20 G. E. Eperon, V. M. Burlakov, P. Docampo, A. Goriely and H. J. Snaith, *Adv. Funct. Mater.*, 2014, **24**, 151.
21 R. F. Service, *Science*, 2013, **342**, 794.
22 Q. Wang, Y. Shao, Q. Dong, Z. Xiao, Y. Yuan and J. Huang, *Energy Environ. Sci.*, 2014, DOI: 10.1039/C4EE00233D.
23 W.-J. Yin, T. Shi and Y. Yan, *Appl. Phys. Lett.*, 2014, **104**, 063903.
24 Y. Shao, Z. Xiao. Q. Dong, Q. I. Wang, C. Bi and J. Huang, unpublished.
25 H. J. Snaith, *Energy Environ. Sci.*, 2012, **5**, 6513.
26 V. Shrotriya, G. Li, Y. Yao, T. Moriarty, K. Emery and Y. Yang, *Adv. Funct. Mater.*, 2006, **16**, 2016.
27 H. J. Snaith, A. Abate, J. M. Ball, G. E. Eperon, T. Leijtens, N. K. Noel, S. D. Stranks, J. T.-W. Wang, K. Wojciechowski and W. Zhang, *J. Phys. Chem. Lett.*, 2014, **5**, 1511.